Hindawi
Shock and Vibration
Volume 2024, Article ID 8849689, 18 pages
https://doi.org/10.1155/2024/8849689

Research Article

Damping Coefficient Optimization for the Articulated System of Virtual Track Trains

Chao Li, Yuanjin Ji, Youpei Huang, Han Leng, Maozhenning Yang, and Lihui Ren

Institute of Rail Transit, Tongji University, Shanghai 200000, China

Correspondence should be addressed to Yuanjin Ji; jiyuanjin@tongji.edu.cn

Received 18 August 2023; Revised 8 February 2024; Accepted 21 February 2024; Published 29 February 2024

Academic Editor: Iacopo Tamellin

Virtual track trains are a new type of rail transportation because the multisection formation structure leads to more degrees of freedom of the vehicle, which may cause unstable phenomena, such as tailing, cross-swing, and folding, affecting the stability and ride comfort of the vehicle driving. To explore the effect of damping coefficient of the articulated systems on vehicle dynamics performance, a vehicle system dynamics model is established based on the actual parameters of a three-module six-axle virtual track train. According to ISO14791: 2000, select typical working conditions such as straight line, lane change, and 1/4 circle curve, and optimize the damping coefficient of the articulated systems through co-simulation. The study shows that under straight-line conditions, increasing the damping coefficient can effectively suppress the yaw angular acceleration and improve the lateral ride comfort of the vehicle but has little effect on the vertical ride comfort. Under lane change conditions, too large or small damping coefficients will deteriorate the train's lateral stability, and a reasonable damping coefficient will improve the yaw damping ratio of the vehicle and reduce the lateral sway vibration between vehicles. Under the 1/4 circle curve conditions, the additional articulated system damper will reduce the vehicle's curve passing performance. In this paper, the articulation stability of multimodule fully connected vehicles is analyzed and optimized for the first time, and the damping coefficient control strategy is given based on the geometric tracking control method. The research results are of great significance for the parameter selection of virtual track trains' articulated system and the design and development of specialized articulated systems for related vehicles.

1. Introduction

Since 2017, when the CRRC Zhuzhou Institute first proposed the Autonomous Rail Rapid Transit concept, virtual track trains (VVT) have rapidly become a hot spot of attention in the rail transportation industry at home and abroad [1]. As a new transportation system between urban trams and articulated vehicles, it has the advantages of large capacity, high punctuality, low construction and operation cost, energy conservation, environmental protection, intelligence and efficiency, etc., and it has the dual roles of alleviating urban traffic pressure and improving the urban image [2, 3]. Virtual track is a target trajectory relative to traditional steel rails, which is achieved through laying magnetic nails on the road or drawing encoded graphics, combined with vehicle visual perception and magnetic induction technology, to achieve the same load-bearing, guiding, and constraint functions as tangible tracks. Virtual track trains utilize path tracking control technology to achieve high-precision autonomous tracking of target paths by controlling the wheel angles of each axle and the driving torque of the drive wheels [4, 5]. Virtual track trains have operational characteristics such as dedicated right-of-way, high-speed dragging driving in straight sections (40–70 km/h), i.e., rear axles locking without steering, low-speed controlled driving in curved sections (10–30 km/h), i.e., full wheel steering, and no emergency lane change. However, different research institutions in China do not seem to have a unified perception of virtual track train architecture, such as CRRC Zhuzhou Electric Locomotive Research Institute Co., Ltd., which released three-module six-axle Autonomous Rail Rapid Transit (ART) in 2017 [6], and CRRC Nanjing Puzhen Co., Ltd., which released three-module eight-axle Digital Rail Rapid Transit (DRT) in 2020. CRRC Zhuzhou Locomotive Co., Ltd. released four-module six-axle Super Autonomous

Rail Rapid Transit (SRT) in 2021 (see Figure 1). The articulated system and the form of damping used between vehicles vary from train to train; for example, DRT uses articulation similar to trams with longitudinal dampers, while ART and SRT use unidirectional or bidirectional disc articulated systems similar to articulated buses.

Disc articulated systems are generally used in low-floor articulated vehicles equipped with hydraulic dampers on each side. They can effectively improve the overall dynamic performance of the vehicle by suppressing the lateral sway and roll motions [7–9]. Scholars worldwide have conducted relatively little research on disc-articulated systems and have mainly focused on damping control and structural design. Liu and Jin [10, 11] used AMESim software to establish a simulation model of the damper of the articulated bus system, and the influence of each structural parameter of the throttle relief valve on the speed-load characteristics of the damper was analyzed by controlling the variables to provide a basis for the subsequent structural optimization of the damper. Szumilas et al. [12] designed a multisensor-based rotating articulated hydraulic damping control algorithm and verified that the control algorithm could improve the train driving stability under right-angle curves and lane change conditions. Cai et al. [13] designed a new type of articulated system that provides both damping and elastic moment between vehicles by adding compression coil springs to the hydraulic arms on both sides of the articulated system. Using the established nonlinear dynamics model of BRT steering motion and the mechanics model of the articulated system, the effects of the damping and stiffness parameters of the articulated system on the dynamic performance of bus steering are analyzed. Xu [14] utilized the reverse design method to establish a flexible body model of the BRT articulated system and analyzed the impact of the articulated system on the handling stability of the bus through the ADAMS vehicle dynamics model. Guan [15] used the dual variables of vehicle speed and articulated disc rotational speed to control the damping of articulated systems through the logic threshold method and established a UM dynamic model for multiarticulated vehicles. The effectiveness of the damper control strategy was verified through co-simulation. He [16] established a four-module six-axle virtual track train UM dynamics model. Still, the articulated system damping was only optimized for straight line driving conditions at different speeds, so the optimization results have limitations on the final damping optimization scheme of the vehicle. Intervehicle dampers are mainly applied between articulated vehicles and high-speed EMUs. The role played is similar to that of articulated system dampers; thus, their findings are of reference significance for the optimization study of disc articulated systems. Vazquez-Vega et al. [17] set articulated dampers between the tractor and semitrailer and found that articulated damping has a significant effect on the lateral acceleration, yaw rate, and rearward amplification of the combined vehicle through the integrated articulated damper kinematic model and the nonlinear yaw-plane model of the train. Qiao et al. [18, 19] developed a 100% low-floor light rail vehicle model using SIMPACK software, simulated semiactive intervehicle longitudinal dampers using the Simulink control module, and found that semiactive dampers with secondary damping could improve both the linear running quality and curve passing performance of the train. Based on the actual parameters of CRH380B EMUs, Sun et al. [20] established a train dynamics model with the same formation method as the actual model. The train's ride comfort, stability, and curve passing performance were calculated and analyzed using the damping and node stiffness of intervehicle longitudinal dampers as the research objects. Shi et al. [21] built a high-speed EMU dynamics model in the SIMPACK environment to study the intervehicle longitudinal damper unloading speed and unloading force and analyze their effects on the EMU's stability, ride comfort, and safety. The above study shows that for articulated vehicles, the low-frequency vibration generated by external excitation and internal structure can be absorbed by setting up intervehicle damping devices, and the tendency of intervehicle folding and lateral sway can be suppressed by the damping torque to improve the running quality and overall vehicle dynamics of the train. As a new type of multiunit articulated vehicle, virtual track trains, in the actual operation of several demonstration lines in China, have problems such as poor ride comfort and poor curve passing performance; therefore, it is of great practical significance to study the parameter optimization of the dampers of the articulated system of virtual track trains.

In this paper, a three-section train dynamics model is established based on the actual parameters of a virtual track train. By changing the damping characteristics of the articulated system dampers, their influence on the vehicle dynamics performance is studied. The damping parameters of the train under typical operating conditions are optimized and analyzed.

2. Establishment of the Train Dynamics Model

The virtual track train consists of three vehicle units, with the end vehicle being the motor vehicle and the middle vehicle being the trailer. All suspensions are in the form of nonindependent suspensions, and all axles are steering axles except for axle 1 and axle 6, which are steering drive axles. The vehicle body and axles are coupled by air springs and dampers; each vehicle is coupled by a bidirectional disc articulated system mounted on the lower end of the vehicle body, with the model of articulated system being IK69B.

A coupled dynamics model of the three-module train is established in SIMPACK software, and each vehicle consists of a car body and two nonindependent suspensions. Steering mechanisms are established separately at all axle positions to meet the trajectory control requirements of the train. The vehicle suspension system comprises nonlinear components such as left and right air springs and dampers. The air spring stiffness and damper damping characteristics are given by setting nonlinear parameters. The tire force model is critical to transmitting the road excitation and reflecting the train operation attitude. Using the tire parameter file, the Pacejka Similarity Magic formula tire model is chosen to define its basic physical properties and mechanical characteristics,

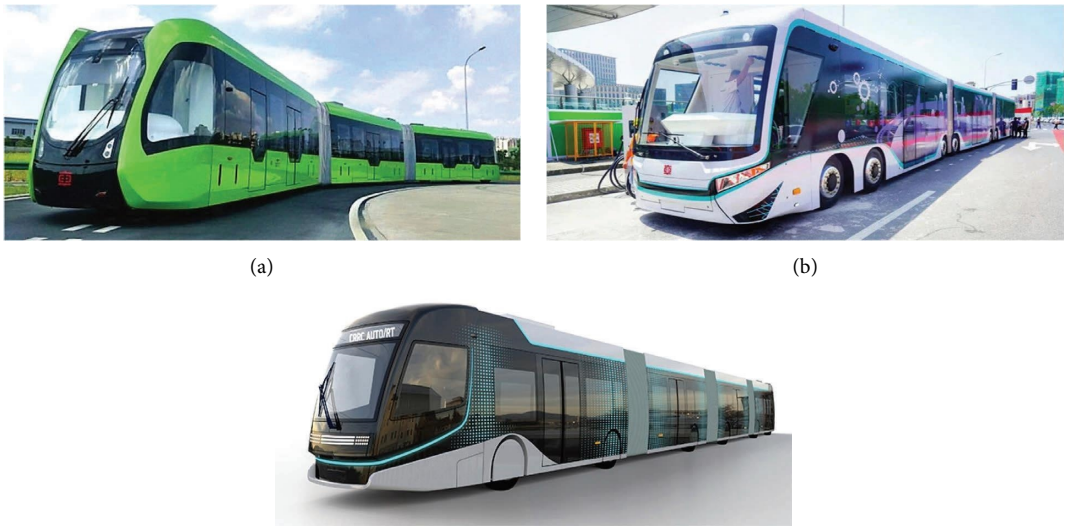

Figure 1: Some virtual track trains in operation. (a) ART. (b) DRT. (c) SRT.

including vertical stiffness and damping, cornering stiffness, and ultimate cornering force, etc. In addition, the model also establishes components such as traction longitudinal tie rods, traction diagonal tie rods, and antiroll torsion bars. The main structural parameters of the vehicle are shown in Table 1.

Through articulated systems, the train realizes coupling, traction, and buffering between vehicles. The two ends of the articulated system model are connected in the center of the lower end of the adjacent car body in the form of hinges to release the nodding degree of freedom. The central hinge constraint is set as a spherical hinge, and the Bushing Cmp force element sets the nonlinear rotational stiffness of the hinge joint to simulate the nodding, rolling, and shaking limits of the central spherical hinge. The left and right damper ends are connected to the front and rear parts of the articulated system. When the adjacent car body undergoes vertical relative rotation, the dampers on both sides will generate recovery and compression damping forces that impede the relative motion, and the Spring-Damper Parallel PtP is used to set the damping parameters of the dampers.

Road surface unevenness is an important factor affecting the dynamic vehicle response [22–24]. This paper adopts the ISO8608: 2016(E) standard to set different road spectrum levels according to different power spectrum density equations. The power spectral density equation is as follows:

$$G_d(n) = G_d(n_0) \cdot \left(\frac{n}{n_0}\right)^{-w}. \quad (1)$$

In the above equation, $G_d(n_0)$ characterizes different pavement roughness classes; n is the spatial frequency with upper and lower values of 2.83 and 0.011 cycles/m, respectively; $n_0 = 0.1$ cycles/m is the reference spatial frequency; and $w = 2$ is the power spectrum density equation fitting index. According to the above principles, the road excitation ISO8608 B and C road spectra are set to simulate the actual running road conditions of the train to the maximum. The train's first axle turning angle is controlled by a closed-loop control system using yaw feedforward and lateral feedback control methods based on the PD lateral controller to simulate the driver's maneuvering, so that the first axle travels according to the target path.

Table 1: Vehicle structure parameters.

Parameters	Value
End vehicle body mass (kg)	11500
Trailer body mass (kg)	13700
Driveshaft axle mass (kg)	750
Steering axle mass (kg)	630
Wheel weight (kg)	105
Tire specification	305/70R22.5
Train length (m)	30.5
Trailer length (m)	9.5
Intervehicle distance (m)	1.4
Floor height (m)	0.32
End vehicle wheelbase (m)	6.2
Trailer wheelbase (m)	6.5

The simulation model of train system dynamics is shown in Figure 2.

3. Articulated System Damper Effect on Train Dynamics Performance

Articulated train dynamics performance evaluation mainly refers to lateral stability, ride comfort, and curve passing performance. The lateral stability evaluation index mainly includes the zero-damping speed under pulse excitation, rearward amplification, and offtracking under lane change conditions, of which the former represents the maximum speed of the stable vehicle operation without lateral sway instability. The ride comfort index is a general evaluation index to evaluate the train operation quality and passenger

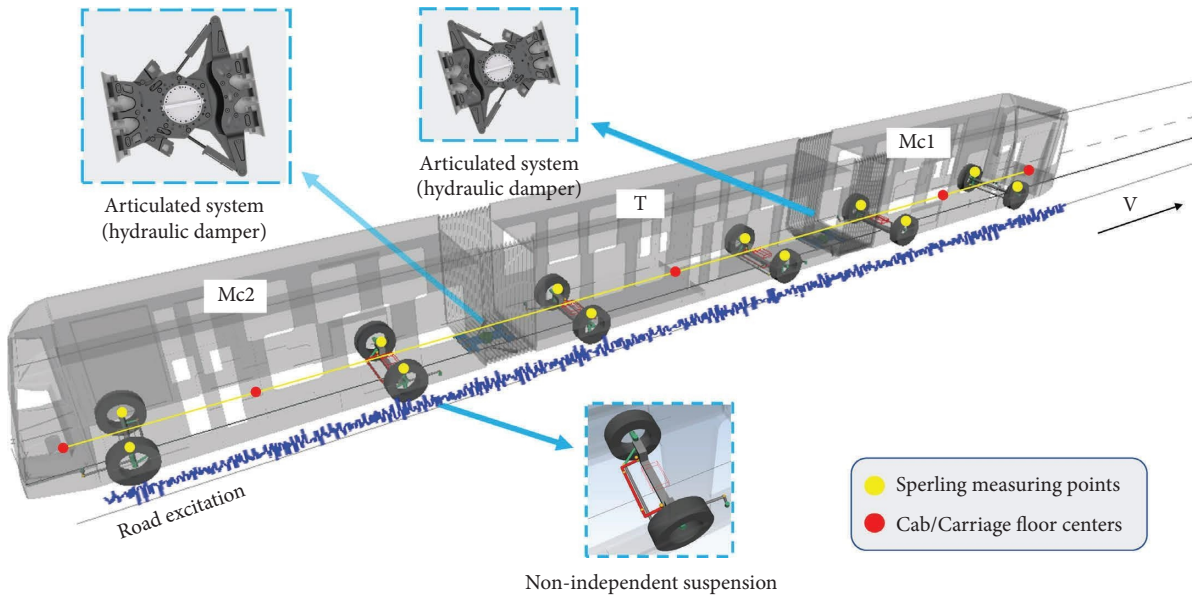

Figure 2: SIMPACK whole vehicle dynamics model.

ride comfort. Among the various ride comfort indexes, the Sperling index is widely used worldwide. The curve passing performance evaluation index includes the minimum turning radius, turning aisle width and tracking deviation. In this paper, based on the established dynamics model, the influence of the articulated system damper damping coefficient on the vehicle dynamics is investigated by varying it under different driving conditions. To simplify the train maneuvering mode, the train is implemented with a tracking control strategy of no rear axles steering at medium and high speeds (>30 km/h) and all-wheel steering at low speeds (≤30 km/h).

3.1. Effect on Lateral Stability. The pulse excitation test can simulate the vehicle's emergency steering, determine the vehicle's lateral sway-damping characteristics due to the steering pulse, and then obtain the zero-damping speed of the train. The pulse test is designed as follows: the train runs at a constant speed on a smooth, unexcited straight road with the rear axles locked. When running for 5 s, a half-cycle sinusoidal input with a frequency of 1 Hz and an amplitude of 4 degrees is applied to the wheel turning angle of the first axle of the vehicle, which excites the head vehicle and the rear vehicle to exhibit lateral sway and determines whether the train is destabilized by observing the convergence of the turning angle of articulated discs. The damping coefficient is a measure of the effectiveness of dampers, reflecting their ability to resist motion, given in units of newton-seconds per meter. The damping coefficients of the damper are changed sequentially to 10^4, 10^5, 10^6, 10^7, and 10^8 Ns/m; the initial speed is 40 km/h and gradually increases with unit speed. When the yaw articulation angle does not converge, determine the zero-damping speed under each damping coefficient. As shown in Figure 3, at a damper damping coefficient of 10^7 Ns/m, the zero-damping speed reaches

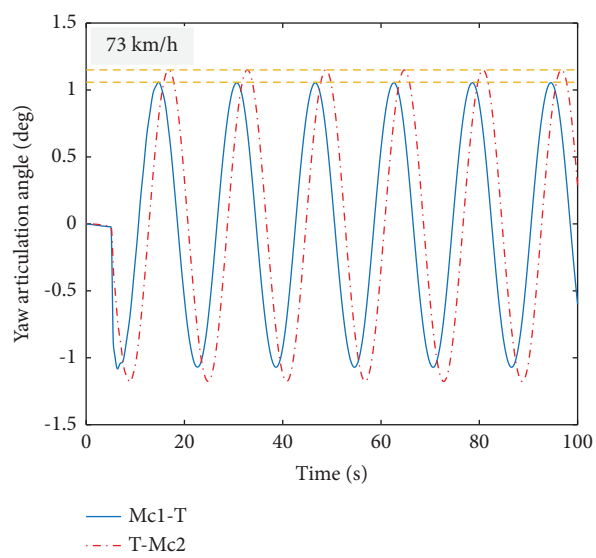

Figure 3: Zero-damping speed at damping coefficient of 10^7 Ns/m.

74 km/h, and the train shows a periodic fixed-amplitude lateral sway motion, which is nonconvergent.

According to the above principles, the zero-damping speeds with different damping coefficients are obtained. To explore the dynamic performance of the train when the articulated system has no damper, a zero damping coefficient is set as a comparison test, and the results are shown in Table 2. It is found that installing a large damping damper can significantly increase the zero-damping speed of the vehicle, and a small damping damper has almost no effect on the zero-damping speed.

The yaw damping ratio is an important indicator reflecting the lateral stability of the articulated train. When the yaw damping is large, the system damping can quickly attenuate the swaying energy of the train to restore the

Table 2: Zero-damping speeds for different articulated damping coefficients.

Damping coefficient (Ns/m)	0	10^4	10^5	10^6	10^7	10^8
Zero-damping speed (km/h)	53	53	54	57	74	84

steady state; in contrast, when the yaw damping is small, it takes a longer time for the train to recover the stable state by small excitation, or even serpentine instability occurs [25, 26]. The response curve of the decaying vibration of the object is shown in Figure 4.

In a small damping system, the damping ratio ζ of this vibration system can be determined when the amplitudes of the two points P and R, separated by N cycles, are measured with the envelope of the amplitude decay curve:

$$\zeta = \frac{\ln \rho}{2\pi N}, \tag{2}$$

where ρ is the amplitude ratio between points P and R, and N is the number of amplitude periods between the two points.

The relationship between the train's yaw damping ratio and vehicle speed under different damping coefficients is calculated, as shown in Figure 5. With different damping coefficients, as the speed increases, the yaw damping ratio of the train gradually drops, and the lateral stability deteriorates. For damping coefficients not exceeding 10^6 Ns/m, the yaw damping ratio is small, the vehicle is prone to instability, and the maximum zero-damping speed is 57 km/h, which is lower than the train design speed of 70 km/h. For damping coefficient values of 10^7 and 10^8 Ns/m, the zero-damping speed reaches 74 and 84 km/h, respectively, which is in line with the train design speed. Therefore, reasonably increasing the articulated system damper damping can improve the vehicle's yaw damping ratio and lateral stability. At the same time, it is also an important parameter to ensure that the train meets the design standards.

Rearward amplification and offtracking are the lateral stability evaluation indexes under the vehicle lane change condition; the former is the ratio of the peak lateral acceleration of the last vehicle unit to the first vehicle unit, and the latter is the maximum lateral displacement of the vehicle first axle midline point trajectory and the last vehicle unit axle midline point trajectory. The lane width is set at 3.5 m, the train runs at the maximum operating speed of 70 km/h on the unexcited road with the rear axles locked, and the influence on the rearward amplification and offtracking of the vehicle is calculated by changing the damper damping coefficient. As seen in Figure 6, the vehicle travels 3.5 m laterally at approximately 9 s to complete the lane change.

Figure 7 depicts the damping coefficient effect on the rearward amplification when the damping coefficient varies from 0 to 10^7 Ns/m. Compared to the uninstalled articulated system damper, when the damping coefficient is less than 10^5 Ns/m, the rearward amplification almost does not change, the lateral acceleration of the car body is the largest, and the train's lateral stability is the worst; when the damping coefficient exceeds 10^5 Ns/m, with the increase in damping, the rearward amplification rapidly decreases, and the lateral stability improves significantly. When the damping is 10^6 Ns/m, the maximum lateral acceleration of the tail car decreases from 2.15 to 1.73 m/s^2, decreasing by 19.5%; when the damping is 10^7 Ns/m, due to the high speed of vehicle lane change, high-frequency rotation is generated between vehicles, and the articulated damping torque is significant. The role of inhibiting the lateral sway of the rear car is highlighted, weakening the backward transmission of the head vehicle lateral instability, resulting in the maximum value of the lateral acceleration of the rear vehicle being smaller than that of the head vehicle, and the rearward amplification is less than 1. When the damping is 10^8 Ns/m, due to the excessive damping of the intervehicle, the vehicle presents a similar rigid connection, which cannot realize high-speed lane changes.

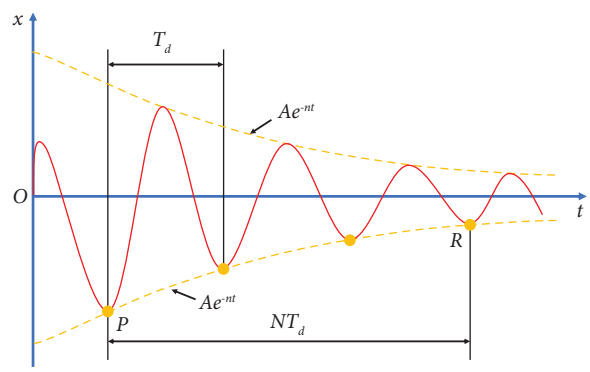

Figure 4: Vibration decay curve.

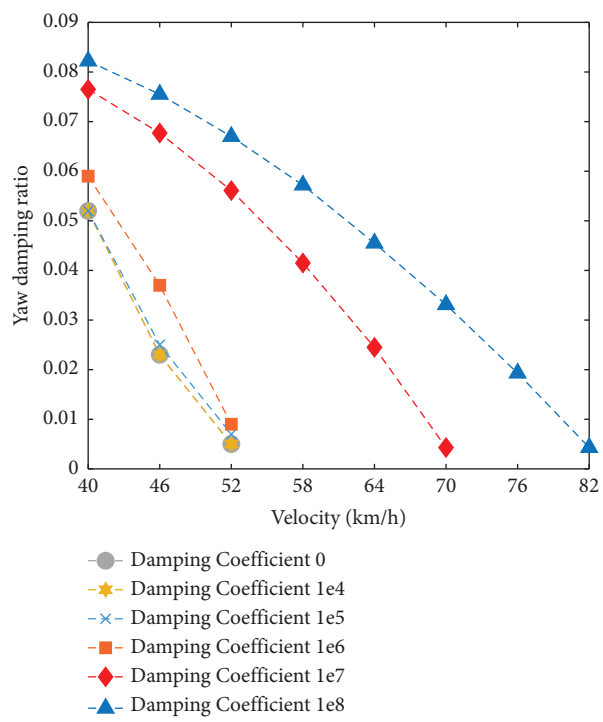

Figure 5: Yaw damping ratio.

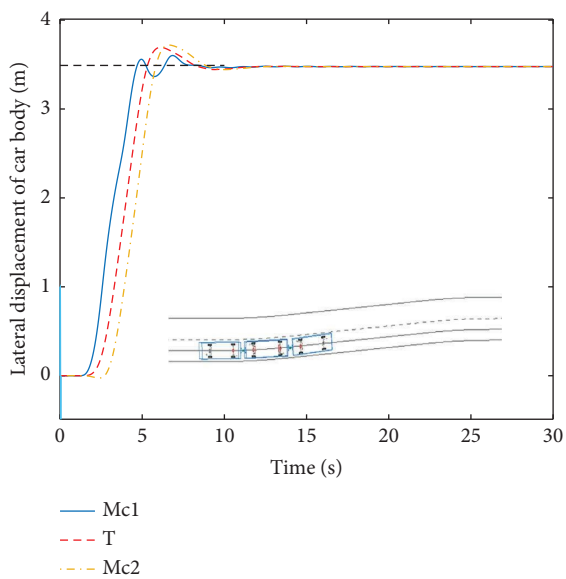

Figure 6: Schematic diagram of lane change.

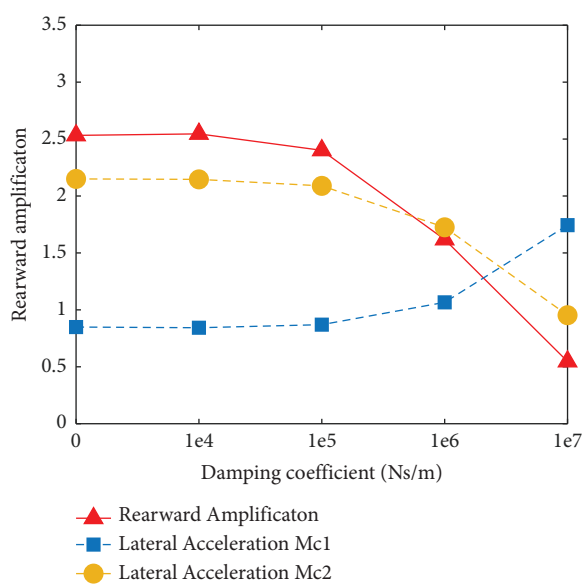

Figure 7: Rearward amplification.

Figure 8 shows the effect of the damping coefficient on the vehicle's offtracking as it varies from 0 to 10^7 Ns/m. As the damping increases, the offtracking shows a decreasing trend similar to the rearward amplification. When the articulated system damper is not installed, the offtracking is the largest, which is 0.724 m; the damping coefficient within the range from 10^4 to 10^5 has little effect on the offtracking; at the damping coefficient values of 10^6 and 10^7 Ns/m, the offtracking significantly drops to 0.634 and 0.511 m, respectively, i.e., by 12.4% and 29.4%, respectively, compared to that without the damper installed. In addition, since the vehicle width is 2.6 m, to ensure that the train does not exceed the lane line, the maximum allowable offset between the axle centerline point and the lane centerline should not exceed 0.45 m. Figure 9 shows the trajectories and

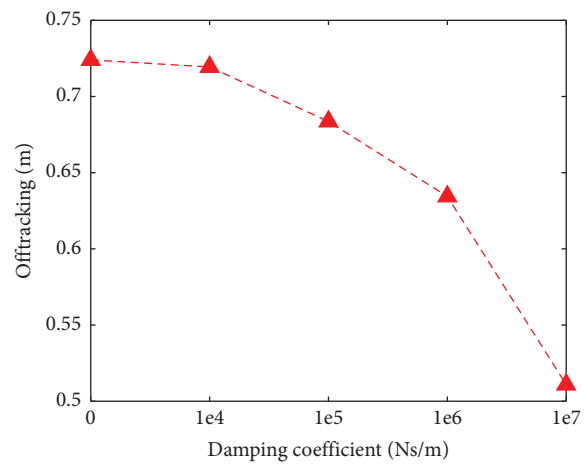

Figure 8: Maximum offtracking.

offtrackings of axle 1, axle 5, and axle 6 for the damping coefficient of 10^7 Ns/m. It can be seen that the offtracking of axle 6 is the maximum, which is 0.304 m; when the damping is 0–10^6 Ns/m, the maximum offtrackings are 0.650, 0.648, 0.633, and 0.549 m, respectively, all exceeding the allowable offset.

Through the above analysis, it can be seen that the damper damping that is too large or too small will worsen the lateral stability of the train. A reasonable damping coefficient should be approximately 10^7 Ns/m, which can not only effectively suppress the lateral instability of the train when it is excited and improve the zero-damping speed but also attenuate the rearward amplification effect of the tail car and ensure that the train is maintained within the lane line when changing lanes.

3.2. Effect on Ride Comfort. The ride comfort index reflects the vehicle's operational quality and passenger comfort. To calculate the Sperling index of the vehicle, the acceleration sensors are set on the floor surface of the carriage at a 1 m transverse deviation of each vehicle unit from the axle center, and the location of the measurement point is shown in Figure 2. Load the ISO8608 B and C road spectra, keep the train running in a straight line at 70 km/h with the rear axles locked, and calculate its effect on the vehicle's lateral ride comfort and vertical ride comfort by changing the damping coefficient.

From Figure 10(a), it is found that the lateral Sperling index of each measurement point tends to improve as the articulated damping increases for both B-class and C-class road spectra. The lateral Sperling index slightly decreases when the damping is 0–10^6 Ns/m and significantly decreases for damping values of 10^7 and 10^8 Ns/m. However, the lateral ride comfort of the head vehicle is always the worst because the front end of the head vehicle is not coupled, and the lateral vibration energy cannot be effectively absorbed. This phenomenon improves with articulated damping greater than 10^6 Ns/m. The Sperling index mean characterizes the average value of the train's ride comfort at all measurement points. For the B-class road spectrum and the

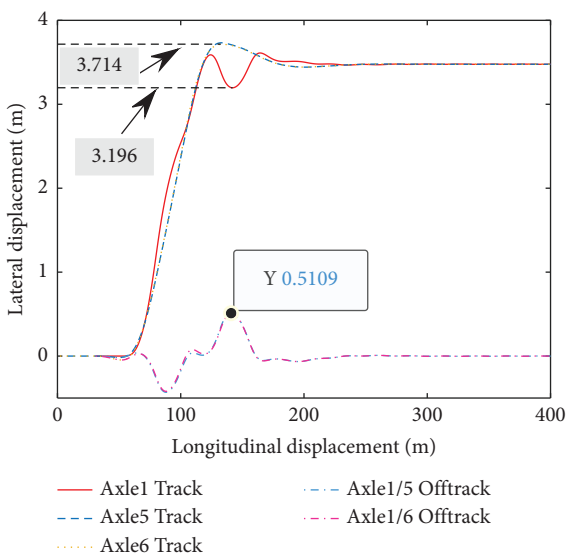

Figure 9: Trajectories and offtrackings of axle 5/6 from axle1.

damping values of 10^7 and 10^8 Ns/m, the Sperling index means are reduced by 14.1% and 18.3%, respectively, compared to not installing an articulated system damper. For the C-class road spectrum and the damping values of 10^7 and 10^8 Ns/m, the Sperling index means, compared to the noninstalled articulated damper, are reduced by 8.2% and 11.8%, respectively, and the lateral ride comfort was optimized from qualified to good and excellent.

Figure 10(b) illustrates the calculated vertical ride comfort of trains with different damping coefficients for B-class and C-class road spectra, and it is found that under different excitation conditions, as the damping increases, the Sperling index of each measurement point shows a trend of improvement, but the optimization effect is not significant. Similarly, for C-class road spectrum and damping values of 10^7 and 10^8 Ns/m, the Sperling index means decreases from 3.11 to 3.02 and 2.99, being improved by 2.9% and 3.9%, respectively.

The above analysis found that the articulated system damper is an essential factor affecting vehicle ride comfort, especially lateral ride comfort. As the articulation damping increases, the vehicle lateral Sperling index continues to decrease, while it can improve the vertical ride comfort to a certain extent. According to the optimization results, the upper limit of the adjustable damping value of the articulated system damper is suitable for straight line conditions.

Figure 11 shows the power spectrum analysis of the yaw angular acceleration of each vehicle unit without the articulated system damper and with the damper damping of 10^7 Ns/m (both horizontal and vertical coordinates are logarithmic coordinates) under B-class road spectrum and 70 km/h operating conditions. From the frequency domain analysis, reasonable damper damping significantly suppresses the yaw angular acceleration near the main frequency of 0.9 Hz.

In Figure 12, the lateral offset of the rear axle of each vehicle unit is calculated under different damping coefficients and vehicle speeds. The variation pattern of each axle is roughly the same, and the lateral offset increases with increasing vehicle speed. The lateral offset is insensitive to the change in the damping coefficient for speeds of 30–40 km/h; for speeds of 50–70 km/h, the lateral offset decreases significantly as the damping increases.

The above results indicate that the Sperling index of the vehicle is negatively correlated with the articulated system damper damping when driving in a straight line at medium and high speeds. As the damping coefficient increases, the Sperling index decreases, at the same time, the lateral offset of the vehicle gradually decreases.

3.3. Effect on Curve Passing Performance. To ensure the smooth passage of the vehicle through the circular curve, an open-loop trajectory control method is used to realize the wheel steering control of the 2–6th axles. Based on the vehicle structural and design parameters, the steering angles of the other axles are calculated by geometric graphical derivation with the first axle turning angle and the two articulated discs turning angles as known quantities.

The kinematic model of the train monorail is shown in Figure 13. The vertical line of the first axle intersects with the angle bisectors of the complementary angles of the angles between vehicle units at points O_1 and O_2; set the wheel turning angle of the sixth axle δ_6 as 1/2 of the angle γ_2 and its vertical line intersects with the angle bisector of the angle γ_2 at point O_3. Therefore, the instantaneous speed centers O_1, O_2, and O_3 of the three vehicle units are obtained. The vehicles' speed instantaneous centers and two to five axles are connected in turn, and vertical lines are made, from which the wheel turning angles (δ_2–δ_5) of each axle can be determined. Through the installation of angle sensors to obtain the first axle wheel rotation angle as well as the angles between vehicle units, and according to the vehicle wheelbase and other structural parameters, the wheel rotation angles of each axle are deduced as follows:

$$\begin{cases} \delta_2 = \arctan\left(\dfrac{|AB| \cdot \tan\gamma_1/2 - |BH_1| \cdot \tan\delta_1}{|AB| + |BH_1|}\right), \\ \delta_3 = \arctan\left(\dfrac{(|CD| + |CH_1|) \cdot \tan\gamma_1/2 - |CH_1| \cdot \tan\gamma_2/2}{|CD| + 2|CH_1|}\right), \\ \delta_4 = \arctan\left(\dfrac{(|CD| + |DH_2|) \cdot \tan\gamma_2/2 - |DH_2| \cdot \tan\gamma_1/2}{|CD| + 2|DH_2|}\right), \\ \delta_5 = \arctan\left(\dfrac{|EH_2| - |EF|}{|EH_2| + |EF|} \cdot \tan\dfrac{\gamma_2}{2}\right), \\ \delta_6 = -\dfrac{\gamma_2}{2}. \end{cases} \tag{3}$$

The above open-loop trajectory control method is established in the Simulink integrated environment, the time delay between the control system and the first axle actuation is set to 0.6 s, and the angle conversion between the

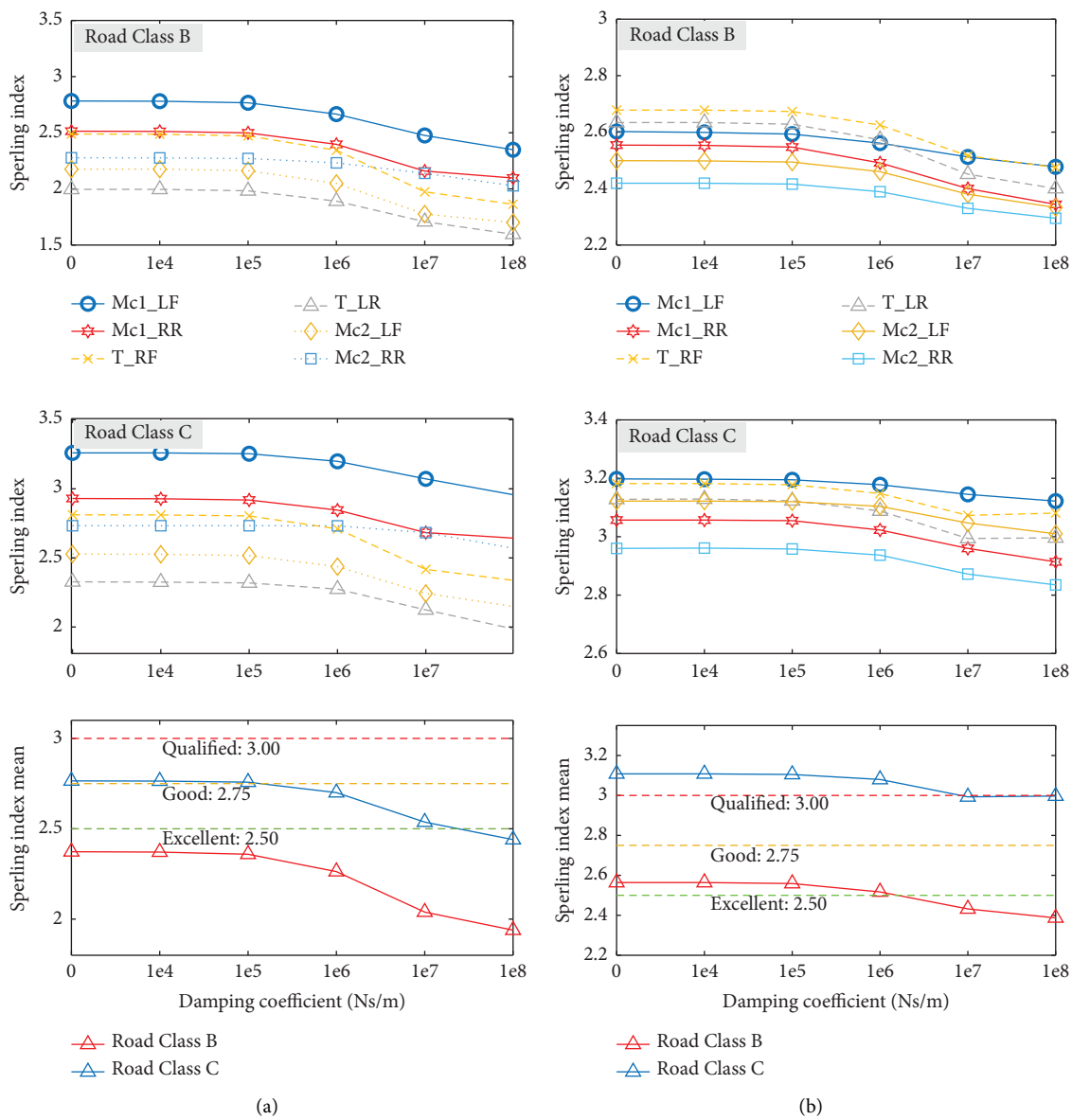

Figure 10: Sperling index. *Note*. LF stands for left front; RF stands for right front; LR stands for left rear; RR stands for right rear. (a) Lateral. (b) Vertical.

theoretical angle calculated by the monorail model and the actual wheel angle is completed. Finally, the angle information of each axle is input into the SIMPACK vehicle dynamics model to complete the co-simulation of vehicle coordinated tracking control. The process is shown in Figure 14.

Set the curve radius to 40 m for the round curve right angle bend, and keep the train running at 20 km/h on a smooth, unexcited straight road. Figure 15 shows the relationship between the horizontal projection of the dynamic envelope of each vehicle unit and the lane line when the articulated system damper damping is 0. From the partial diagram, it can be seen that the envelope of the car body will cross the lane line when the train is in and out of the circular curve, and there is a danger of the train occupying other lanes or colliding with other objects. To avoid danger, widened sections are usually set on both sides of a specific curve position, or the trajectory control model of the train is optimized to reduce the running limit of the vehicle further, so that the dynamic envelope of the train is strictly kept within the lane lines on both sides. According to the operation line design specification, it is proposed to set the widened sections on both sides of the road in the curve section. At the same time, it is required that the dynamic envelope width should not exceed 4.5 m when the train passes through R30–R60 right angle turns.

To facilitate observation of the effect of damping coefficients on the turning aisle width, the dynamic envelope is expanded along the target path, as shown in Figure 16. The vehicle drifts to the inside of the lane when entering the circular curve and to the outside of the lane when exiting the circular curve, and as the damping increases, the tendency of

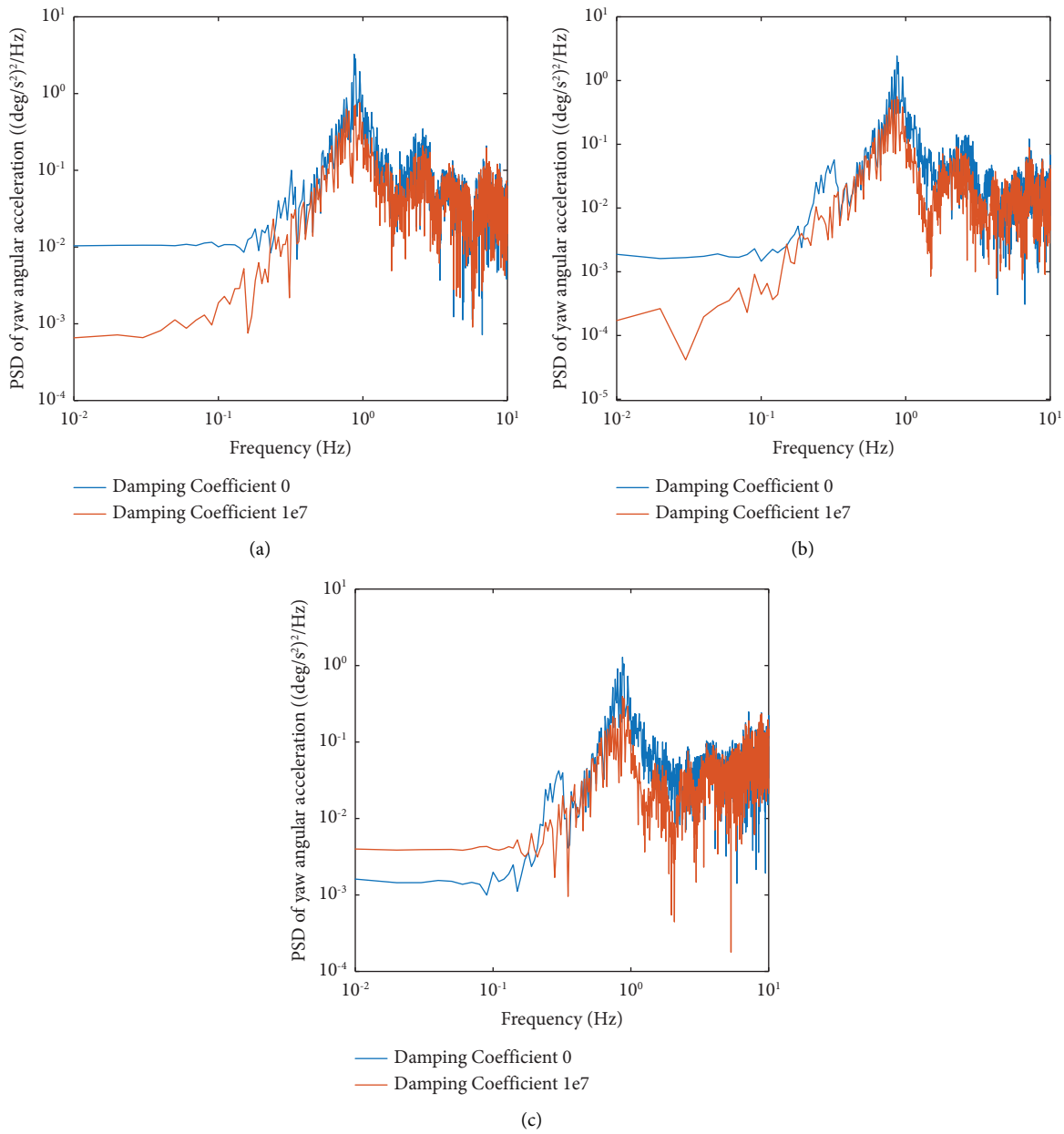

Figure 11: Power spectrum of yaw angular acceleration. (a) Mc1. (b) T. (c) Mc2.

the vehicle to deviate from the target path increases, and the curve passing performance worsens. Figure 17 shows the variation curve of the dynamic envelope width along the route travel direction, and the result shows that at zero damping, the aisle width is the smallest, namely, 3.575 m. At a damping value below 10^5 Ns/m, it almost does not affect the aisle width. At damping values of 10^6 and 10^7 Ns/m, the turning aisle width values are 3.622 and 3.961 m, respectively. Compared with no damper damping, the aisle width increases by 1.3% and 10.8%, respectively, and the curve passing performance tends to deteriorate. Through the above analysis, it is preliminarily judged that setting the articulated system dampers will reduce the curve passing performance of the vehicle.

4. Optimization Analysis of Damper Damping for Articulated Systems

The vehicle's articulated system adopts semiactive damping control technology, which can determine the operating conditions by collecting real-time information such as the vehicle speed, rotation angle, and rotational angular velocity of articulated discs, thereby controlling the output of the damping force [27]. The reasonable matching of damper damping for different operating conditions and speeds is an important guarantee to give full play to the articulated system's role and improve train's dynamic performance [28]. Road class, operating speed, and damping coefficient of the articulated systems are important factors that affect the

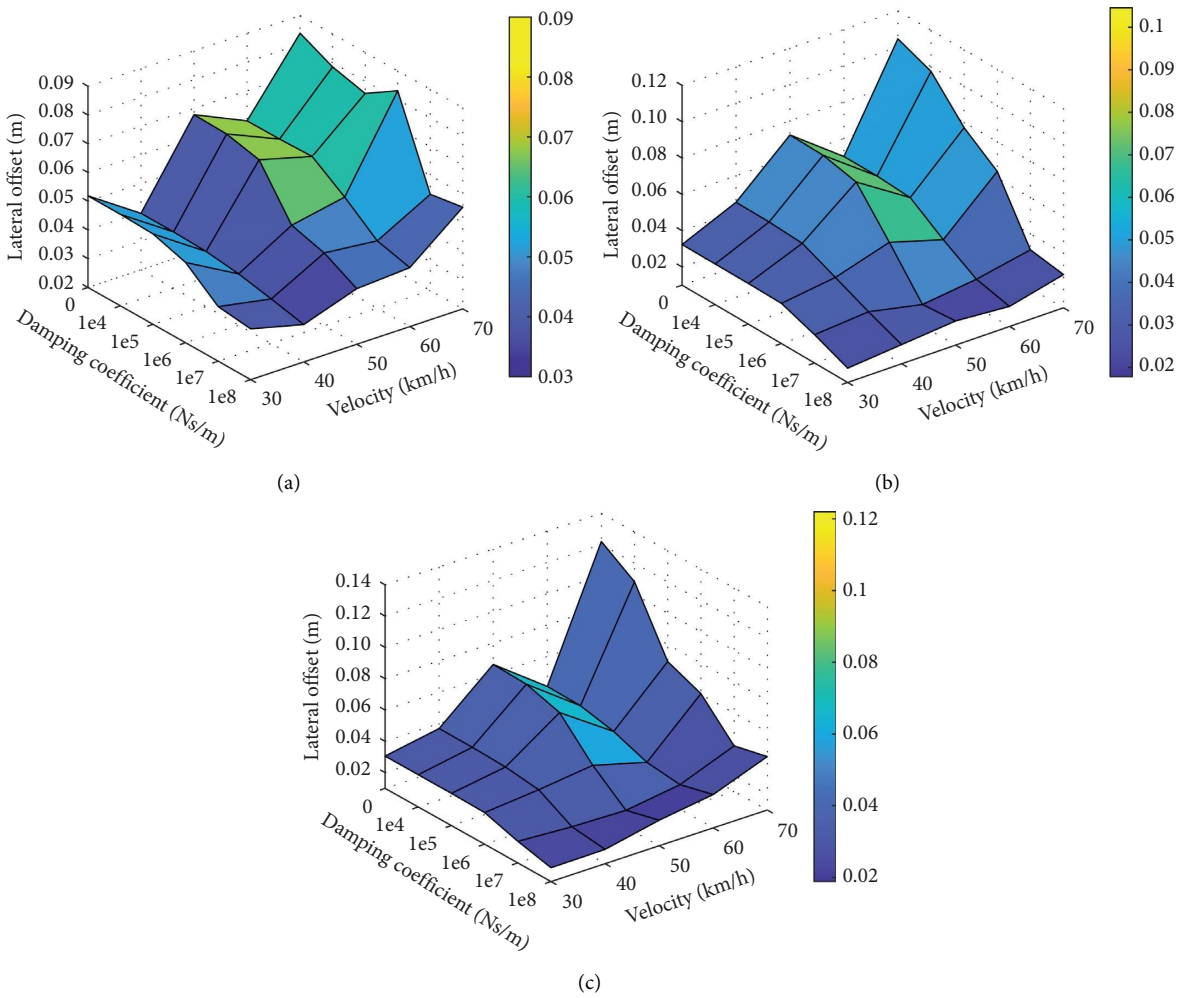

Figure 12: Lateral offset of axles. (a) Axle2. (b) Axle4. (c) Alxe6.

simulation results. Considering that the actual operating conditions of the vehicle are mostly limited to urban fixed planning lines, this section uses Design of Experiments (DOE) approach, selects the operating speed and damping coefficient of the articulated systems as two factors, and adopts full factorial design to conduct dynamic optimization analysis under straight line, lane change, and 1/4 circle curve conditions.

4.1. Straight Line Condition. The road surface unevenness is set as B-class road spectrum, and the vehicle runs in a straight line at 30–70 km/h with the rear axles locked. According to the analysis results in Section 3.2, select the damping optimization range of 0–10^8 Ns/m and calculate the effect of different articulated system damper damping on the vehicle ride comfort. The results show that the lateral Sperling index mean improves at different speeds as the articulated damping increases, especially when the vehicle is running at medium and high speeds. For damping coefficients exceeding 10^7 Ns/m, the lateral Sperling index will be significantly reduced, and the optimization effect is good. The vertical Sperling index mean decreases with increasing articulated damping at different speed levels, and the improvement effect is not pronounced compared with lateral ride comfort. As seen in Figure 18, the upper limit of the adjustable damping value of the articulated system damper should be used for the straight line condition.

4.2. Lane Change Condition. The lane change route is the same as in Section 3.1, setting the road surface unevenness as B-class road spectrum, train running speed of 30–70 km/h, and rear axles locked. According to the above analysis results and the adjustable interval of actual damping, the optimized damping range is determined to be from 10^6 to 5×10^7 Ns/m. To fully respond to the influence of damping changes on the lateral stability of the train, the rearward amplification and the lateral offset of all axles relative to the target path are selected as evaluation indexes.

Figure 19 shows the effect of the damping coefficient on the rearward amplification at different speeds. At 30 km/h, the lateral acceleration of both end vehicles increases with increasing damping, and the rearward amplification shows an increasing trend. At 40 km/h, when the damping is less than 2×10^7 Ns/m, the rearward amplification is not sensitive to the

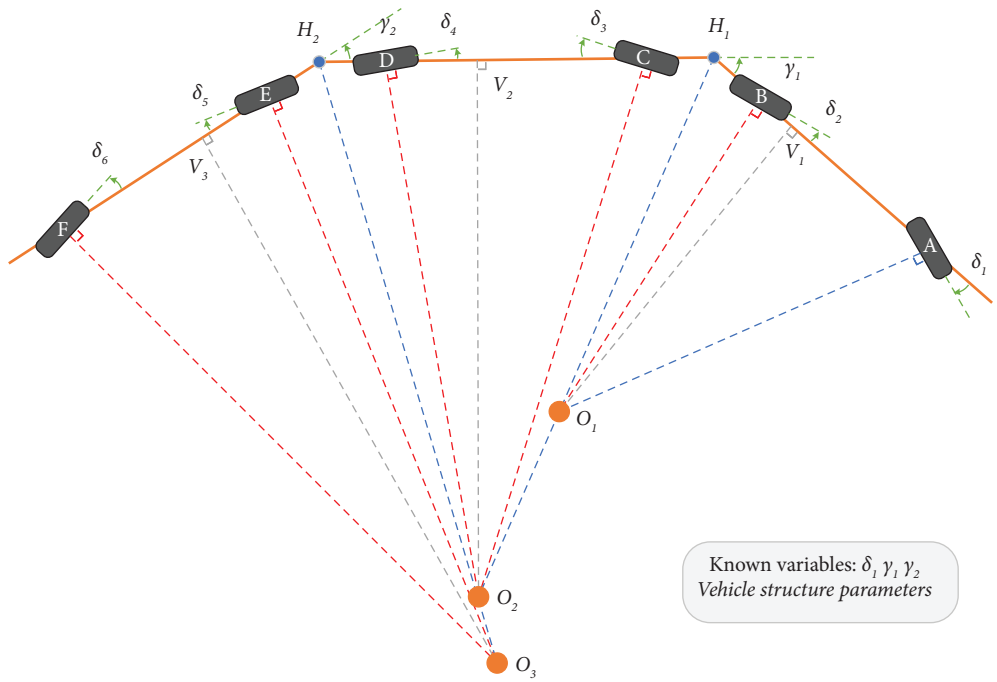

Figure 13: Vehicle monorail kinematic model.

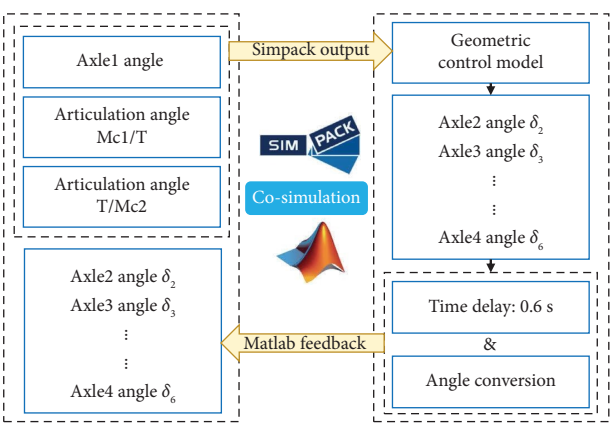

Figure 14: SIMPACK/Simulink cosimulation model.

change in damping and is less than 1; when the damping exceeds 2×10^7 Ns/m, the rearward amplification increases rapidly, but the overall lateral acceleration of the end vehicles remains at a low value. At 50–60 km/h, the rearward amplification shows a decreasing trend with increasing damping, and the decreasing trend is apparent near 2×10^7 Ns/m. However, when the damping exceeds 2×10^7 Ns/m, the lateral acceleration of the head vehicle unit increases significantly. At 70 km/h, the rearward amplification decreases with increasing damping. For damping coefficients exceeding 4×10^6 Ns/m, the rearward amplification is less than 1, the lateral acceleration of the head vehicle increases gradually with increasing damping, and the change tends to slow down after the damping reaches 10^7 Ns/m.

Figure 20 illustrates the damping coefficient effect on the lateral offset of each axle at different speeds. At 30 km/h, the lateral offset of all axles is the smallest at zero damping. At 40–50 km/h, when the damping is less than 10^7 Ns/m, the lateral offset is insensitive to the change in damping. At a damping of 2×10^7 Ns/m, the lateral offset appears to be a minimum; when the damping exceeds 2×10^7 Ns/m, the lateral offset of each axle increases rapidly as the damping increases. At 60–70 km/h, except for the first axle, the lateral offset of all axles decreases with increasing damping and decreases to the lowest level when the damping increases to 2×10^7 Ns/m.

Based on a comprehensive analysis of the calculation results of the rearward amplification and the lateral offset of axles, it is concluded that under lane change conditions at vehicle speeds below 30 km/h, it is not appropriate to set dampers' damping; within the speed range of 40–70 km/h, it is recommended to set dampers' damping of 2×10^7 Ns/m.

4.3. 1/4 Circle Curve Condition. The 1/4 circle curve route and the vehicle tracking control strategy are the same as in Section 3.3. The road surface unevenness is set as B-class road spectrum, the operating speed is 10–40 km/h, and the articulated damping range is selected as 0–10^7 Ns/m. The effect of damper damping on the turning aisle width is calculated by co-simulation. The results show that at 10–30 km/h, the turning aisle width of the vehicle remains the smallest, and the curve passing performance is the best at zero damping coefficient. With the increased vehicle speed and damping, the turning aisle width increases, and the calculation results are shown in Table 3. The turning aisle width at 40 km/h does not meet the train design requirements.

Figure 21 illustrates the damping coefficient effect on the lateral offset of the tail axle relative to the target path at different speeds. The results also show that the lateral offset of the vehicle's tail axle is minimized at a damping coefficient

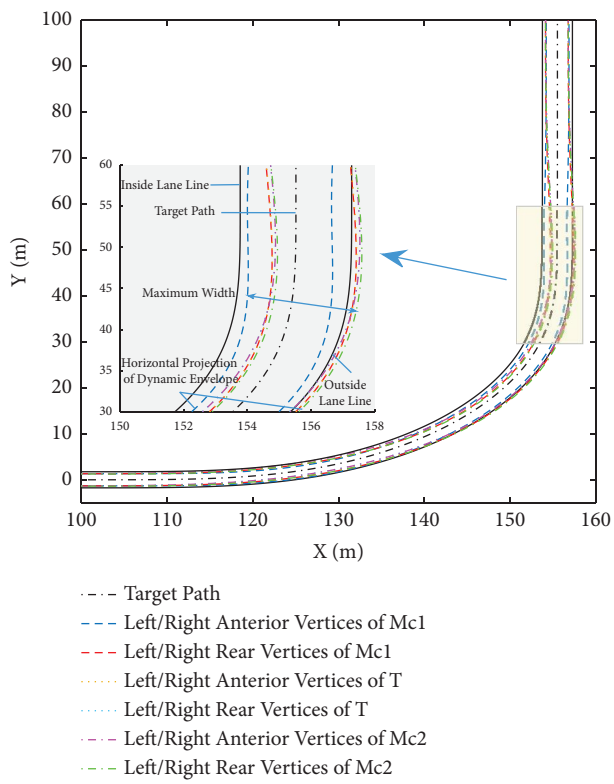

Figure 15: Vehicle dynamic envelope.

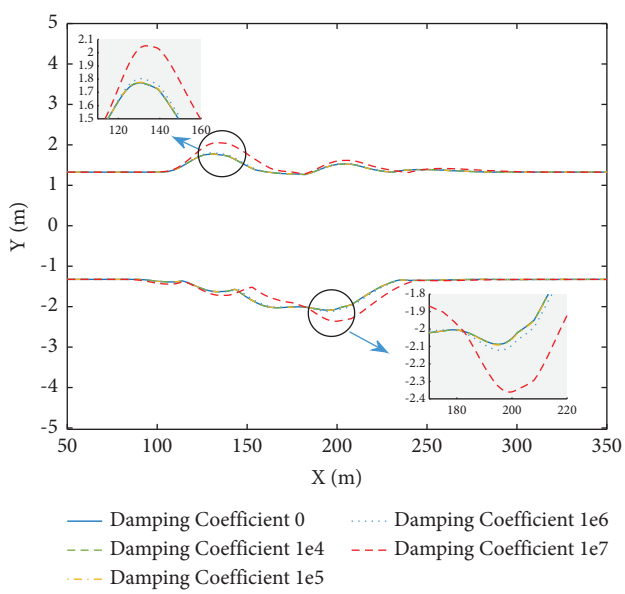

Figure 16: Dynamic envelope expansion along the path.

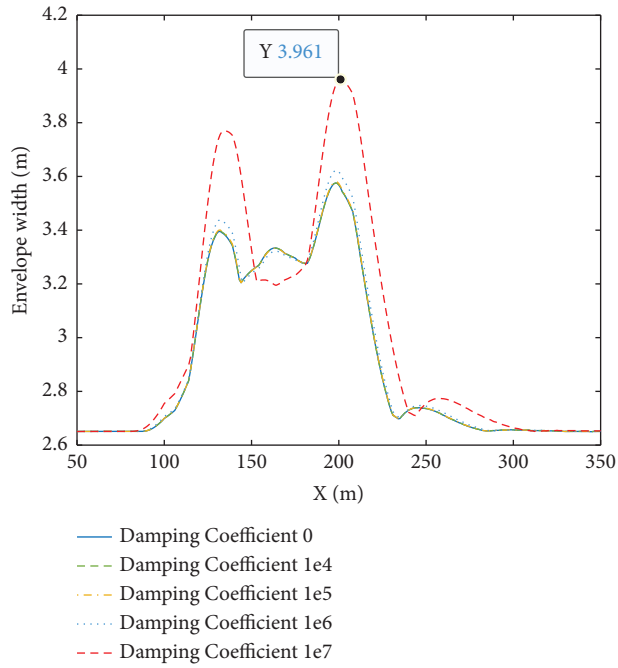

Figure 17: Variation curve of envelope width along the path.

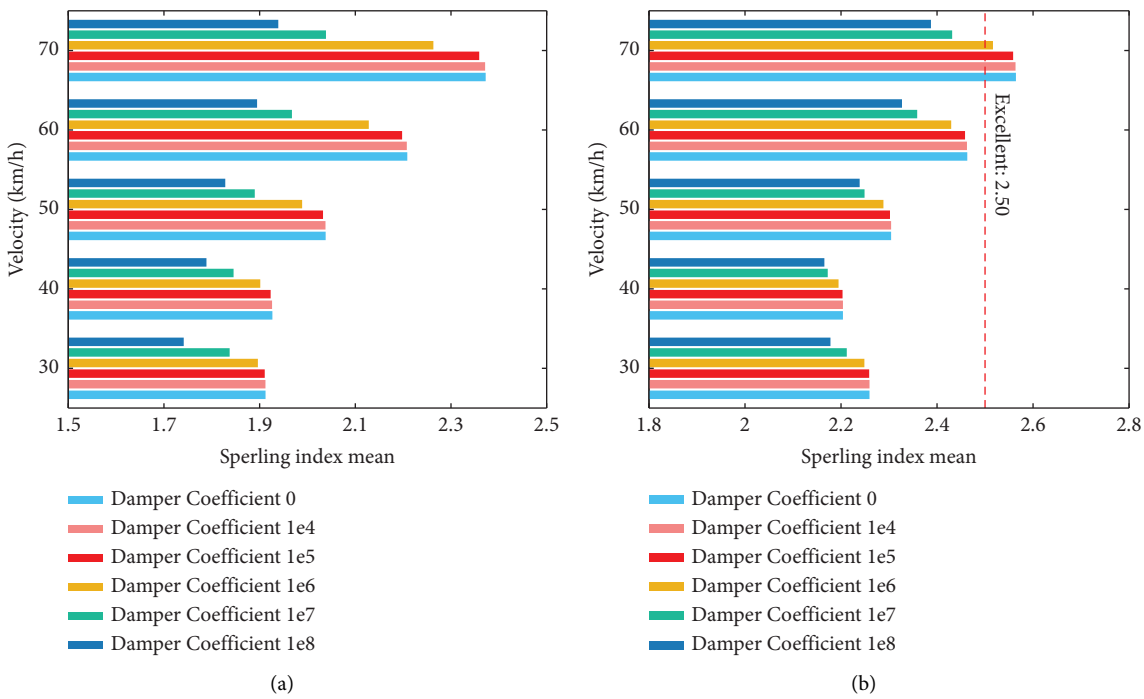

Figure 18: Sperling index. (a) Lateral. (b) Vertical.

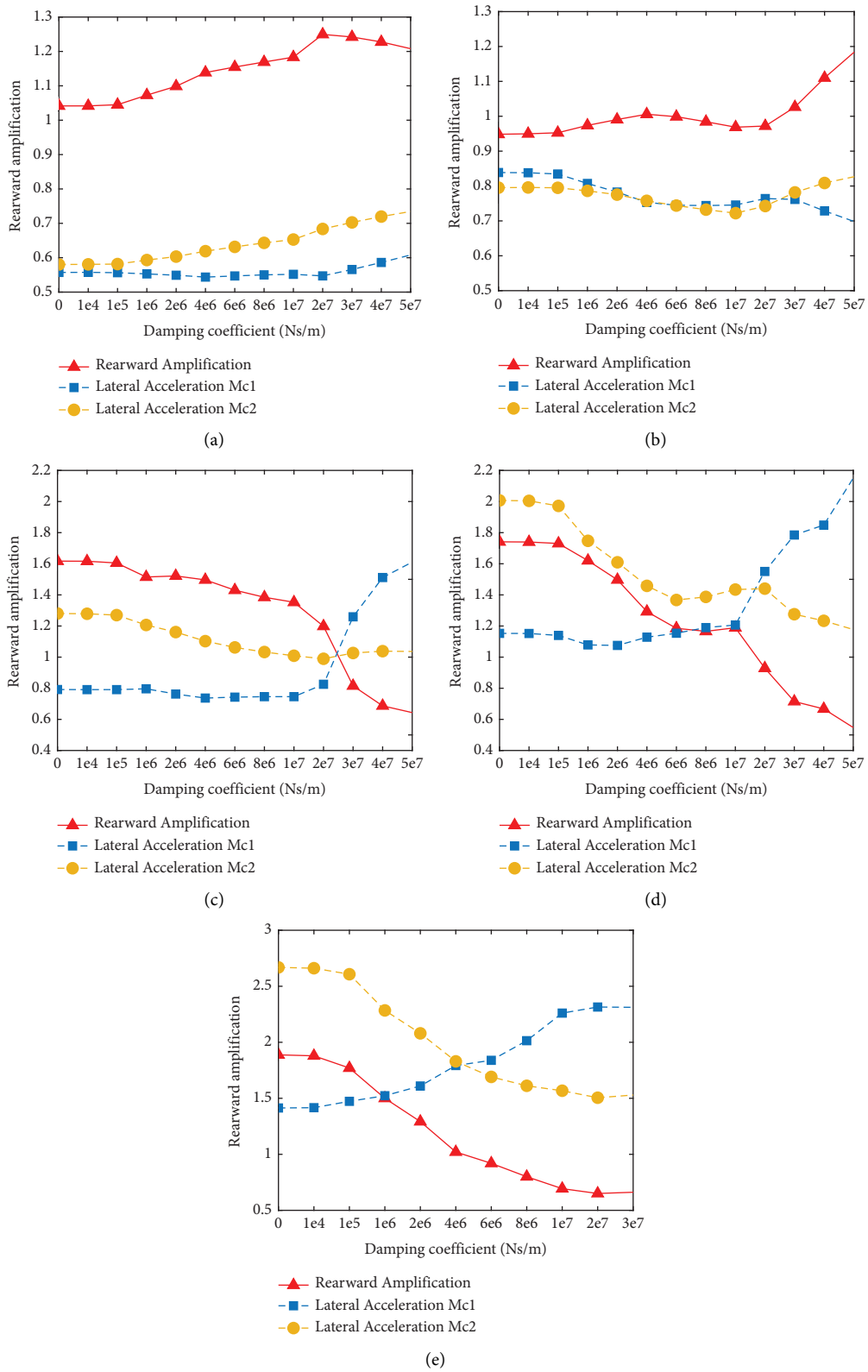

Figure 19: Rearward amplification. (a) 30 km/h. (b) 40 km/h. (c) 50 km/h. (d) 60 km/h. (e) 70 km/h.

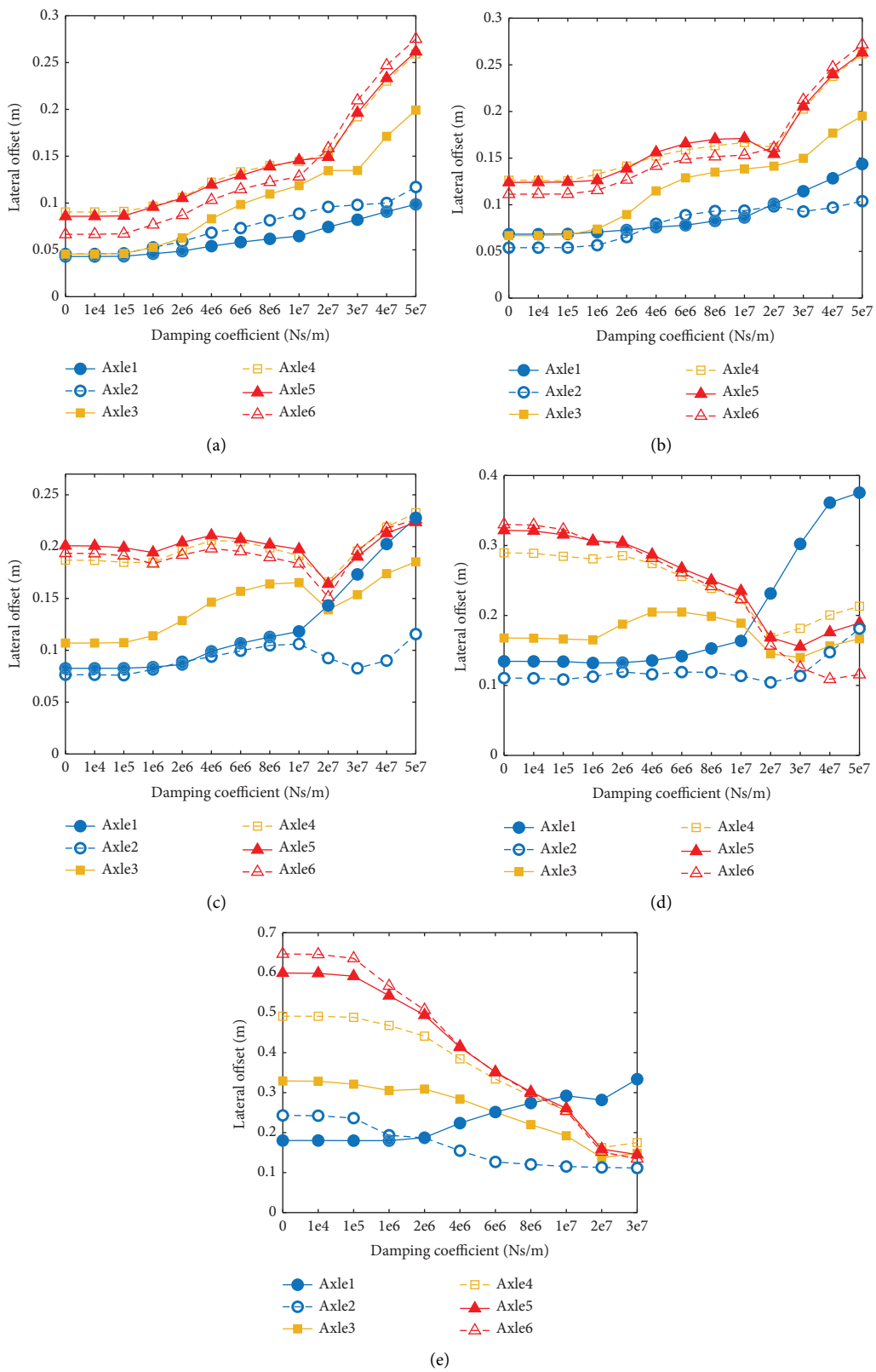

Figure 20: Lateral offset. (a) 30 km/h. (b) 40 km/h. (c) 50 km/h. (d) 60 km/h. (e) 70 km/h.

Table 3: Effect of articulated damping on turning aisle width.

Speed (km/h)	Damping coefficient (Ns/m)				
	0	10^4	10^5	10^6	10^7
10	3.587	3.587	3.590	3.612	3.805
20	3.571	3.573	3.576	3.620	3.963
30	3.725	3.725	3.726	3.718	4.172
40	5.450	5.446	5.412	5.174	—

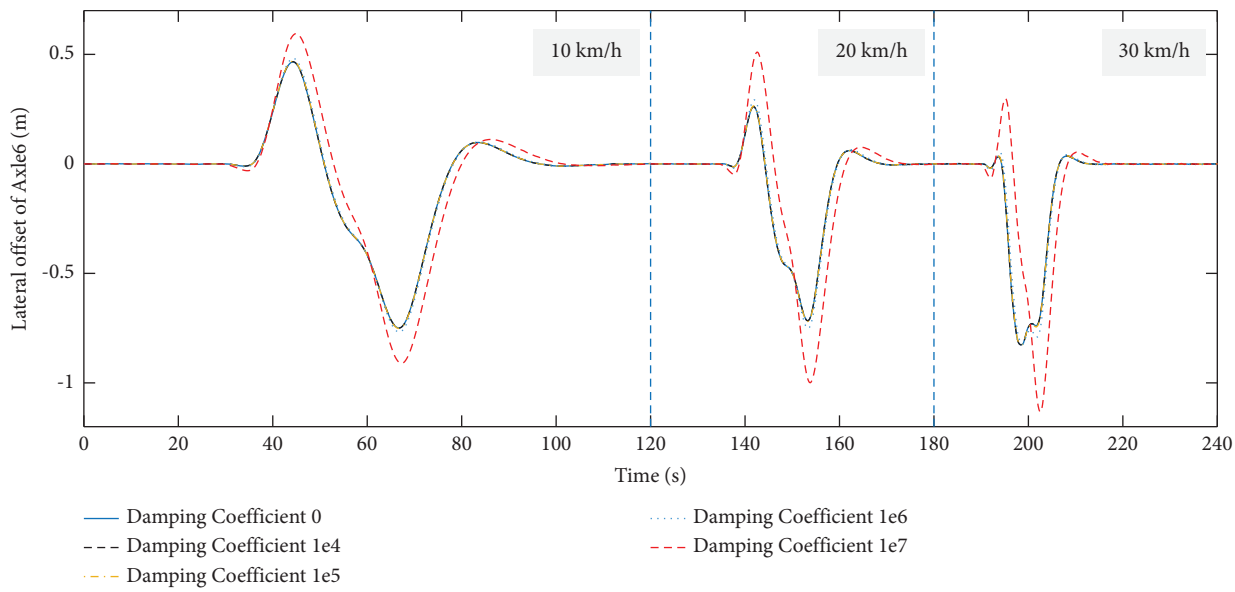

Figure 21: Lateral offset of the tail axle.

of zero. In summary, the vehicle should pass through the small curve section at speeds below 30 km/h and without articulated system damper damping.

5. Conclusions

This paper adopts the actual parameters of a three-module six-axle virtual track train, considers the tire and suspension systems' nonlinearity, and establishes a coupled multibody dynamics model of a three-module train. Taking the damper damping of the articulated system as the research object, the lateral stability and ride comfort of the vehicle are analyzed and optimized. A tracking control model for all-wheel steering of vehicles is established using geometric graphical methods. The train's curve passing performance is analyzed and optimized through SIMPACK/Simulink co-simulation. The research results show that reasonable matching of articulated damper damping for different driving conditions and speeds can effectively improve the overall dynamic performance of the vehicle. The following conclusions can be drawn as follows:

(1) The damping coefficient of the articulated system damper is the critical parameter affecting the virtual track train's lateral stability, ride comfort, and curve passing performance.

(2) If the train is not equipped with articulated system dampers or the dampers' damping is small, the yaw damping ratio of the train is relatively small, which is prone to serpentine instability. Appropriately increasing the articulated damping can improve the yaw damping ratio and effectively enhance the zero-damping speed of the vehicle. With damping coefficient of 10^7 Ns/m, the zero-damping speed exceeds the maximum design operating speed, reaching 74 km/h and exceeding that without articulated dampers by 39.6%.

(3) Too large or small damper damping coefficients will deteriorate the vehicle's lane change performance. If the damping coefficient is too small, the train's lateral oscillation cannot be effectively suppressed, and the rearward amplification and offtracking evaluation index are poor. If the damping coefficient is too large, the vehicle units are connected quasi-rigidly, and a high-speed lane change cannot be achieved.

(4) The vehicle ride comfort is optimized with increasing damper damping, especially the lateral ride comfort. The calculation results show that the damping coefficient of 10^7 Ns/m has a significant suppression effect on the yaw angular acceleration of the vehicle body near the main frequency of 0.9 Hz. When the

vehicle operates at high speed in the C-class road spectrum, a reasonable damping coefficient can make the lateral Sperling index of the train excellent. The damper damping has little effect on the vertical dynamic performance of the train.

(5) The small damping damper has almost no effect on the train curve passing performance. As the damping increases, the turning aisle width of the train increases, and the curve passing performance worsens.

Based on the optimization results of this paper, the following recommendations on damping coefficients for different operating conditions are given: Under straight line conditions, using the upper limit of the adjustable damping of the articulated system dampers is recommended. Under lane change conditions, at motion speeds below 30 km/h, articulated damping is not recommended. Within the speed range of 40–70 km/h, the recommended articulated damping coefficient is 2×10^7 Ns/m. Under 1/4 circle curve conditions, articulated damping is not recommended. In this paper, the full factorial experimental design method is used to reasonably match the damping coefficients under typical working conditions, providing an important reference for the parameter selection of the articulated system of virtual track trains and the optimization development of damping control strategies for the articulated system.

Data Availability

The data used to support the findings of this study are available from the corresponding author upon request.

Conflicts of Interest

The authors declare that they have no conflicts of interest.

Acknowledgments

This research was financially supported by the National Natural Science Foundation of China (Grant no. 52205121).

References

[1] Y. J. Zhang, "Research on system mode and applicability of medium carrying-capacity urban rail transit in China," Master's Thesis, Beijing Jiaotong University, Beijing, China, 2021.

[2] K. Wang, S. Ma, J. L. Chen, F. Ren, and J. B. Lu, "Approaches, challenges, and applications for deep visual odometry: toward complicated and emerging areas," *IEEE Transactions on Cognitive and Developmental Systems*, vol. 14, no. 1, pp. 35–49, 2022.

[3] L. G. Yan, "Development and application of the maglev transportation system," *IEEE Transactions on Applied Superconductivity*, vol. 18, no. 2, pp. 92–99, 2008.

[4] H. Leng, L. H. Ren, and Y. J. Ji, "Cascade modular path following control strategy for gantry virtual track train: time-delay stability and forward predictive model," *IEEE Transactions on Vehicular Technology*, vol. 71, no. 7, pp. 6969–6983, 2022.

[5] Z. H. Wang, Z. G. Lu, J. Y. Wei, and X. J. Qiu, "Research on virtual track train path-tracking control based on improved mpc and hierarchical framework: a reconfigurable approach," *Applied Sciences*, vol. 13, no. 14, p. 8443, 2023.

[6] S. Liu, C. Li, T. Yuwen, Z. L. Wan, and Y. P. Luo, "A lightweight lidar-camera sensing method of obstacles detection and classification for autonomous rail rapid transit," *IEEE Transactions on Intelligent Transportation Systems*, vol. 23, no. 12, pp. 23043–23058, 2022.

[7] F. Vlk, "Lateral stability of articulated buses," *International Journal of Vehicle Design*, vol. 9, no. 1, pp. 35–51, 1988.

[8] A. D. Felice, M. Mercantini, and S. Sorrentino, "Stability analysis of articulated bus in straight-ahead running manoeuvre," *Applied and Computational Mechanics*, vol. 7, no. 3, pp. 1649–1662, 2021.

[9] T. L. Lei, J. X. Wang, and Z. W. Yao, "Modelling and stability analysis of articulated vehicles," *Applied Sciences*, vol. 11, no. 8, p. 3663, 2021.

[10] J. H. Liu and X. J. Jin, "Modeling and simulation of load characteristics of passenger car hinged disk damper," *Advances in Materials, Machinery, Electronics III*, vol. 2073, 2019.

[11] J. H. Liu and X. J. Jin, "The influence of the parameters of throttle type overflow valve on thevelctiy load characteristic of the hinged disc damper," *Metrology and Measurement Technique*, vol. 46, no. 9, pp. 8–10, 2019.

[12] M. Szumilas, S. Luczak, M. Bodnicki, M. Stozek, and T. Zaluski, "Method of controlling innovative articulation for articulated vehicle," in *Proceedings of The Xxii Slovak-Polish Scientific Conference On Machine Modelling And Simulations 2017*, Rydzyna, Poland, September, 2018.

[13] Y. M. Cai, Y. L. Jiang, S. J. Zhang, and S. A. Chen, "Development and optimisation of an articulation system to improve intersection turning speed of bus rapid transit vehicle," *International Journal of Heavy Vehicle Systems*, vol. 22, no. 3, pp. 213–235, 2015.

[14] B. Xu, "Reversing-design of the articulation systems for BRT vehicles and research of the vehicles' virtual prototyping's simulation," Master's Thesis, Qingdao Technological University, Qingdao, China, 2009.

[15] H. D. Guan, "Multi-articulated road train path tracking with articulated disc variable damping control research," Master's Thesis, Xiamen University of Technology, Fujian, China, 2022.

[16] D. He, *Simulation Research on Running Stability and Ride comfort of Four-Group Virtual Train*, Xihua University, Chengdu, China, 2021.

[17] D. Vazquez-Vega, S. Rakheja, A. K. W. Ahmed, and A. Lozano-Guzman, "Directional performance analysis of an A-train double with externally mounted dampers," *International Journal of Heavy Vehicle Systems*, vol. 8, no. 2, pp. 155–176, 2001.

[18] Y. Qiao and J. Zeng, "Dynamics performance effects of longitudinal damper between the low-floor light rail vehicles," *Machinery*, vol. 11, pp. 17–20+30, 2014.

[19] Y. Qiao, "Dynamic performance lmprovement for low-floor light rail vehicles using semi-active dampers," Master's Thesis, Southwest Jiaotong University, Chengdu, China, 2014.

[20] C. L. Sun, S. X. Zhou, Z. Qin, Y. Sun, and X. H. Zhao, "Research on influence of the characteristic parameter of inter-vehicle longitudinal damper on dynamic performance of high speed EMUs," *Chinese Journal of Mechanical Engineering*, vol. 24, pp. 170–176, 2017.

[21] L. Shi, H. J. Song, Z. T. Guo, J. J. Wu, and C. B. Xu, "Influence of inter-vehicle lonqitudinal damper on dynamic

performance of electric multiple units," *Chinese Journal of Construction Machinery*, vol. 5, pp. 377–381, 2018.

[22] X. Y. Ma, W. W. Quan, Z. J. Dong, Y. K. Dong, and C. Si, "Dynamic response analysis of vehicle and asphalt pavement coupled system with the excitation of road surface unevenness," *Applied Mathematical Modelling*, vol. 104, pp. 421–438, 2022.

[23] C. P. Wang, J. M. Zhang, H. C. Zhou, Z. Xue, M. S. Mei, and H. Y. Lu, "Dynamic load characteristics and road friendliness of virtual track train in full running conditions," *Journal of Tongji University*, vol. 50, no. 6, pp. 871–878, 2022.

[24] Z. H. Yin, J. Y. Zhang, and H. Sui, "Stochastic responses characteristics of a virtual track train excited by road irregularities," *IEEE Transactions on Vehicular Technology*, vol. 71, no. 8, pp. 8152–8163, 2022.

[25] F. P. Bu, H. S. Tan, and J. H. Huang, "Lateral control of an articulated bus for lane guidance and curbside precision docking," in *Proceedings of the 2010 American Control Conference*, pp. 3854–3859, Baltimore, MD, USA, June, 2010.

[26] N. Zhang, T. Li, J. Ma, and G. D. Yin, "The mechanism research of body sway of car-trailer combinations considering steering system characteristics," *Advances in Dynamics of Vehicles on Roads and Tracks*, Springer Nature, Berlin, Germanypp. 1435–1446, 2020.

[27] T. Xu, Y. H. Shen, Y. J. Huang, and A. Khajepour, "Study of hydraulic steering process for articulated heavy vehicles based on the principle of the least resistance," *IEEE/ASME Transactions on Mechatronics*, vol. 24, no. 4, pp. 1662–1673, 2019.

[28] S. A. Chen, B. B. Gu, F. Qiu, R. He, and C. Li, "Influence of velocity change on handling and stability of vehicle," *Journal of Traffic and Transportation Engineering English Edition*, vol. 2, pp. 60–65, 2009.